Acta Pharmaceutica Sinica B 2021;11(11):3493−3507

Chinese Pharmaceutical Association
Institute of Materia Medica, Chinese Academy of Medical Sciences

Acta Pharmaceutica Sinica B

www.elsevier.com/locate/apsb
www.sciencedirect.com

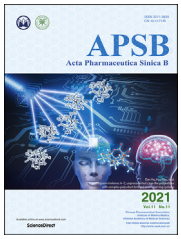

ORIGINAL ARTICLE

Ginsenoside Rg1 ameliorates blood−brain barrier disruption and traumatic brain injury *via* attenuating macrophages derived exosomes miR-21 release

Kefeng Zhai[a], Hong Duan[a,e,*], Wei Wang[a,d], Siyu Zhao[a], Ghulam Jilany Khan[f], Mengting Wang[a], Yuhan Zhang[a], Kiran Thakur[b], Xuemei Fang[a], Chao Wu[a], Jianbo Xiao[c,*], Zhaojun Wei[b,*]

[a]*Suzhou Engineering Research Center of Natural Medicine and Functional Food, School of Biological and Food Engineering, Suzhou University, Suzhou 234000, China*
[b]*School of Food and Biological Engineering, Hefei University of Technology, Hefei 230009, China*
[c]*Department of Analytical Chemistry and Food Science, Faculty of Food Science and Technology, University of Vigo-Ourense Campus, Ourense E-32004, Spain*
[d]*School of Biological and Food Engineering, Anhui Polytechnic University, Wuhu 241000, China*
[e]*Key Laboratory for Chemistry and Molecular Engineering of Medicinal Resources (Guangxi Normal University), Guilin 541004, China*
[f]*Department of Pharmacology and Therapeutics, Faculty of Pharmacy, University of Central Punjab, Lahore 54000, Pakistan*

Received 7 January 2021; received in revised form 5 March 2021; accepted 12 March 2021

KEY WORDS

Traumatic brain injury;
Exosome;
MiRNA-21;
Blood−brain barrier;
Ginsenoside Rg1;
Nonmuscle myosin IIA

Abstract During the traumatic brain injury (TBI), improved expression of circulatory miR-21 serves as a diagnostic feature. Low levels of exosome-miR-21 in the brain can effectively improve neuroinflammation and blood−brain barrier (BBB) permeability, reduce nerve apoptosis, restore neural function and ameliorate TBI. We evaluated the role of macrophage derived exosomes-miR-21 (M-Exos-miR-21) in disrupting BBB, deteriorating TBI, and Rg1 interventions. IL-1β-induced macrophages (IIM)-Exos-miR-21 can activate NF-κB signaling pathway and induce the expressions of MMP-1, -3 and -9 and downregulate the levels of tight junction proteins (TJPs) deteriorating the BBB. Rg1 reduced miR-21-5p content in

*Corresponding authors. Tel./fax: +86 557 2871037, +86 551 62901539.
E-mail addresses: szxydh@163.com (Hong Duan), jianboxiao@uvigo.es (Jianbo Xiao), zjwei@hfut.edu.cn (Zhaojun Wei).
Peer review under responsibility of Chinese Pharmaceutical Association and Institute of Materia Medica, Chinese Academy of Medical Sciences.

https://doi.org/10.1016/j.apsb.2021.03.032

IIM-Exos (RIIM-Exos). The interaction of NMIIA−HSP90 controlled the release of Exos-miR-21, this interaction was restricted by Rg1. Rg1 could inhibit the Exos-miR-21 release in peripheral blood flow to brain, enhancing TIMP3 protein expression, MMPs proteolysis, and restricting TJPs degradation thus protected the BBB integrity. Conclusively, Rg1 can improve the cerebrovascular endothelial injury and hold the therapeutic potential against TBI disease.

1. Introduction

Traumatic brain injury (TBI) poses a major risk of infirmity and death accompanied by long-term grave neurological impairment in the central nervous system (CNS) of survivors[1,2]. TBI may be the primary cause of mechanical stress or secondary in nature due to the pathophysiological disruptive changes in blood−brain barrier (BBB), cell apoptosis, inflammatory responses, free radical production, and excitotoxic damage[3]. These changes evolve within minutes to months after the primary injury[1]. It has been reported that BBB disruption is due to disconnection of cerebrovascular endothelial cells (ECs) from integrated vascular system *via* intercellular tight junctions (TJs)[4]. This disruption of BBB further takes part in deterioration of microenvironment of normal neuronal physiology[1].

Exosomes (Exos) with a diameter of 30−150 nm are endogenous nanovesicles responsible for cell-to-cell transmission by transporting functional molecules of central dogma[5]. Some transport proteins (*e.g.*, TSG101 and HRS), lipids (*e.g.*, ceramide), and tetraspanins (*e.g.*, CD63 and CD9) have been confirmed to control multivesicular bodies (MVB) biogenesis and exosome secretion[6]. Nonmuscle myosin IIA (NMIIA) participates in the stage wise cytoskeletal reform that is vital for lytic granule release[7−9]. However, the role of NMIIA for exosome regulation in TBI still remains unstated. Lately, studies have identified that exosomes can voluntarily cross the BBB and act as delivery vehicles with a possible role to deliver explicitly designed components to CNS[10]. These transferred exosomes can modify the brain structure and its functionality, and may offer a preferable approach for the TBI disease interventions[11].

As small non-coding RNA molecules, microRNAs (miRNAs, miRs) induce translation repression or mRNA degradation[12,13]. The dysregulation of miRNAs in TBI models has been evidently reported several times in previous studies[11,14,15]. Clinical and basic research findings have shown that miR-21 expression was improved both in the brain cortex after TBI and cultured neurons after scratch injury[11,14,15]. Furthermore, exosomes miRNA are known to facilitate the neuroinflammation and neuronal injury[14,16,17].

Ginsenoside Rg1, as a major biomolecule, is mainly responsible for the pharmacological activities (neurotrophic and neuroprotective) of ginseng[18−20]. Nevertheless, findings from pharmacokinetic studies indicated that ginsenoside Rg1 cannot be proficiently transported across the BBB[21−23]. Moreover, the machinery by which ginsenoside Rg1 "lessens" TBI *in vivo* is still not fully explored. In this study, we hypothesize that ginsenoside Rg1 can suppress the secretion of exosome-miR-21 *via* NMIIA as key regulator besides improving the effect of cerebral vascular endothelial injury, protecting the integrity of the BBB, and thus plays a central role in prevention and treatment of cerebral vascular disease.

2. Materials and methods

2.1. Reagents

IL-1β and blebbistatin were procured from PeproTech Inc. (NJ, USA) and Selleckchem (Houston, TX, USA), respectively. Ginsenoside Rg1, dimethyl sulfoxide (DMSO), and anti-HSP90 antibody were acquired from Sigma−Aldrich (St. Louis, MO, USA). Primary antibodies against TIMP3, HSP90, p-P65, and P65 were obtained from Cell Signaling Technology (Beverly, MA, USA). ZO-1, occludin, claudin-5, TSG101, and GFAP were procured from Abcam (Cambridge, MA, USA). Antibody against NMIIA was purchased from Proteintech (Wuhan, China). Antibodies against MMP-3, MMP-9, CD6, CD9, VEGF, GAPDH and β-actin were acquired from EnoGene BIO Inc. (Nanjing, China). Secondary antibodies conjugated with horseradish peroxidase (HRP) were obtained from Bioworld Technology Inc. (St. Louis Park, MN, USA). MMP-1 antibody was acquired from Boster Biological Technology (Wuhan, China). Enhanced chemiluminescene (ECL) reagents, RIPA lysis buffer, and protease inhibitor were procured from Vazyme Biotech (Nanjing, China).

2.2. Cells culture

After procurement from American Type Culture Collection (Manassas, VA, USA), primary human brain microvascular endothelial cells (HBMECs) and human myeloid leukemia mononuclear cells (THP-1 cells) were respectively cultured in supplemented Dulbecco's modified Eagle's medium (DMEM; Gibco Laboratories, Grand Island, NY, USA) and RPMI1640 (Gibco Laboratories) followed by incubation at 37 °C in a 5% CO_2 humidified atmosphere.

2.3. Preparation and isolation of exosomes

THP-1 cells were seeded into the dishes at appropriate density and differentiated into macrophages[24] after treatment with 100 ng/mL phorbol-12-myristate acetate (PMA) (Sigma−Aldrich, Missouri, USA) for 24 h. Cell morphology was characterized by phase contrast microscopy (Olympus CKX31, Tokyo, Japan). Then, time dependent IL-1β (20 ng/mL) treatment was given [with or without Rg1 or blebbistatin (1 μmol/L)] to macrophages. Subsequently, the supernatants were collected and purified by ultracentrifugation of exosomes as described previously[25], *i.e.*, normal macrophages (NM-Exos), IL-1β-induced macrophages (IIM-Exos), IL-1β-

induced macrophages + Rg1 (RIIM-Exos), and IL-1β-induced macrophages + blebbistatin (BIIM-Exos). Briefly, the above supernatant was centrifuged at 1000×*g* and then at 10,000×*g* for 20 min in order to get rid of cell debris. After obtaining the purified exosomes, they were passed through a 0.22 mm filter followed by ultracentrifugation at 100,000×*g* to pellet exosomes. The exosome-enriched fraction was then washed with phosphate buffer saline (PBS) and then centrifuged twice at 100,000×*g*. Finally, the purified exosome fraction was re-suspended in PBS and were quantified by BCA protein assay kit for further use. NM-Exos, IIM-Exos, RIIM-Exos, and BIIM-Exos were quantified to 100 μg/mL for each cell groups.

2.4. Evaluation of exosomes through transmission electron microscopy

According to earlier described study[26], in order to examine the morphology of IIM-Exos, 20 μL of Exos was fixed over a carbon-coated copper grid (Nisshin EM, Co., Ltd., Tokyo, Japan) for 5 min followed by staining with 2% uranyl acetate and drying for 10 min. Finally, the stained grids were pictured with transmission electron microscope (Tecnai G2 Spirit TEM, Zeiss, Oberkochen, Germany) at 120 kV.

2.5. Identification of exosomes by nanoparticle tracking analysis

Size distribution of Exos (diluted with deionized water to 1.0 mL) was tracked on the basis of Brownian movement and diffusion coefficient using Nanoparticle Tracking Analysis (NTA, Nano-Sight NS300, Malvern, Worcestershire, UK)[27] using blank medium and deionized water as references.

2.6. Western blot analysis

Lysates of cells, exosomes, and tissues and dilutions of quantified proteins were arranged following the previous methods[28,29]. After resolving the protein samples (30 μg) on SDS-polyacrylamide gel electrophoresis (SDS-PAGE), they were shifted to polyvinylidenedifloride (PVDF) films. The loaded membranes were blocked with 5% skimmed milk and incubated with primary and secondary antibodies for over-night at 4 °C and 2 h at room temperature, respectively. Immunoreactive protein bands and their intensities were visualized under the FluorChem HD2 Imaging system (Protein Simple, CA, USA) and Alpha View SA, respectively.

2.7. TaqMan quantitative RT-PCR

For the RT-PCR, total RNA was extracted (Haigene Biotech, Haerbin, China) and quantified (NanoDrop 2000 Spectrophotometer, Thermo-Fisher Scientific, Wilmington, DE, USA). Cell supernatant or plasma exosomal RNAs were used for TaqMan-based miRNA assays in order to measure the expression level of miR-21-5p. After reverse transcription (Haigene Biotech, Haerbin, China), miRNA expression levels were evaluated using qRT-PCR. The detection of mature miRNAs was carried out using MiRcute Plus miRNA qPCR Kit (Haigene Biotech, Haerbin, China) containing a QuantiTect SYBR Green PCR Master Mix and the miScript Universal Primer along with the miRNA-specific primer. Amplified PCR products were detected on a ViiA™ 7 Real-Time PCR System (Applied Biosystems, Foster City, CA, USA). The normalization of the miR-21-5p expression levels was performed using U6 small RNA as an internal control.

2.8. TIMP3 mRNA quantification by qPCR

Total RNA extraction (Life Technologies, Gaithersburg, MD, USA)[28,29] was followed by concentrations (260 nm) and purity determination (280 nm). Reverse transcriptase reactions were prepared using the PrimeScript® RT reagent Kits (Takara, Otsu, Shiga, Japan) and ViiA™ 7 Real-Time PCR System (Applied Biosystems). The qPCR was performed using cDNA fragments treated with SYBR Green RT-PCR (Takara Biotechnology Co., Ltd., Tokyo, Japan) using ViiA™ 7 system and data was analyzed using the $\Delta\Delta C_T$ method and 18S was taken as internal control.

2.9. Exosome precipitation and RNA isolation in serum

For exosomes isolation, ExoQuick (System Biosciences, Mountain View, CA, USA) was used as per the manufacturer's instructions with slight modifications[30]. The isolate was centrifuged at 10,000×*g* for 5 min, and the obtained supernatant was mixed with 125 μL of ExoQuick solution. After incubation at 4 °C overnight, the mixture was centrifuged at 1500×*g* for 30 min. The exosome pellet was dissolved in 25 μL PBS and RNA was extracted using miRNeasy Micro Kit (QIAGEN, Valencia, CA, USA). The obtained RNA was subjected to quantity and quality determinations using the NanoDrop 2000 Spectrophotometer.

2.10. NMIIA knockdown

As reported in our earlier studies[28,29], the sequences of the siRNAs (5′-GAGGCAAUGAUCACUGACUdTdT-3′ and 5′-AGUCAGUGAUCAUUGCCUCdTdT-3′) used to suppress NMIIA expression were designed and produced by Biomics Biotechnologies Co., Ltd. (Nantong, China). After the HBMECs reached 70%−80% confluence, they were transfected with siRNA (100 nmol/L) using ExFect Transfection Reagent and further co-incubated with Exos for designated time.

2.11. In vitro BBB model

The establishment of *in vitro* BBB model was carried out in cell culture inserts, dishes and plates following the previous protocol[31]. Collagen (15 mg/mL) and fibronectin (30 mg/mL) were coated on the trans-well PET membranes (0.4-μm pore, 11-mm diameter; Corning, Lowell, MA, USA) prior to HBMECs seeding. After seeding at appropriate density, cultures were maintained at 37 °C in a 5% CO_2 humidified atmosphere for 3 days to reach confluence enable to form BBB. Subsequently, HBMECs were stimulated macrophage-derived exosomes.

2.12. Tracking of PKH67 labelling of Exos

Exo samples (100 μg) from macrophages were incubated with 230 μL of Diluent C and 2 μL of PKH67 dye (Sigma−Aldrich) as reported previously[32]. After suspension of this mixture for 5 min,

FCS depleted of Exos were added to the Exo mixture to block the staining reaction. Ultra-centrifugation (100,000×*g*) of labeled Exos was followed by the resuspension in PBS and then incubation with HBMECs in dishes for 18 h. In addition, 5-μm sections *in vivo* were incubated with PKH67 dye. Sections were again stained with the above mixture, then the staining reaction was stopped with FCS depleted of Exos. The PKH67 labelling samples were assessed using the confocal microscope (Olympus, Tokyo, Japan).

2.13. TEER measurements

The integrity of the *in vitro* BBB models was evaluated by measuring the trans-endothelial electrical resistance (TEER)[33,34]. The HBMECs were seeded on each insert (upper compartment) in Transwell™ plate and stimulated with 0.1 μg/mL exosomes. The TEER was measured on daily basis using a Millicell® ERS-2 Electrical Resistance System according to manufacturer's protocols. The TEER values of coated but cell-free inserts were subtracted from the measured TEER values, and the difference was multiplied with the size of the insert (0.3 cm^2 for each 24-well insert).

2.14. Measurement of Evens blue albumin

HBMECs were allowed to confluently grow on a porous polyethylene terephthalate Transwell insert for 48 h to mimic the endothelium of the BBB. According to previous studies[34,35], endothelial barrier leakage was detected using the flux of Evans blue dye-labeled albumin (EB-albumin, Sigma) across a HBMECs monolayer. Briefly, after macrophage-derived exosomes treatment, lower section of the well was supplemented with 150 μL of bovine serumal bumin (BSA, 4%), whereas top compartment was filled with 50 μL of EB-albumin solution (2%) 1 h prior to the end of the stimulation. To quantify the migration in the Transwell inserts, absorbance of the medium at a detection wavelength of 620 nm was determined.

2.15. Transfection of miR-21 mimic and inhibitor

After 16 h culturing of the HBMECs in 6-well plates (about 5×10^5 cells/well), transfection was carried out with miR-21 minic (50 nmol/L), or miR-21 inhibitor (100 nmol/L), or their equivalent negative controls. More efficient transfection was ensured with the supplementation of RNAifectin™ transfection reagent (6 μL)[36] followed by the replacement of culture medium to remove the transfection reagent and then, detection after 24 h of transfection. RNAifectin™ transfection reagent and other compounds were purchased from Biomics Biotechnologies Co., Ltd. (Nantong, China).

2.16. Dualluciferase reporter assay

As the 293T cells reached the confluency of 85%−90%, they were co-transfected with 2 μg of pLenti-UTR-GFP vector with human TIMP3-3′UTR and human mutant TIMP3-3′UTR cloned behind the coding sequence and 2 μg of pre-miR-21-5p or negative control in serum- and antibiotics-free DMEM with DNAfectin™ Plus Transfection Reagent (FulenGen, Guangzhou, China) for 6 h[36]. After the medium replacement, the cells were incubated for another 12 h period. *Firefly* and *Renilla* luciferase were measured in cell lysates (FulenGen) on Luminometer 20/20n (FulenGen). The cellular density and transfection efficiency were determined in terms of *Renilla* luciferase.

2.17. Co-immunoprecipitation

The treated THP-1 cells were lysed in a RIPA lysis buffer containing protease inhibitor (Vazyme Biotech, Nanjing, China). Anti-NMIIA antibody (Abcam, USA) together with protein A/G agarose, was used to immunoprecipitate NMIIA and associated proteins. Proteins were resolved by SDS-PAGE and the resulting bands were detected by Western blot analyses or stained with silver staining and then comparatively analyzed to identify specific binding proteins by MALDI-TOF-MS.

2.18. Animals preparation

Adult male Sprague−Dawley (SD) rats were procured from the Yangzhou University (Yangzhou, China) and experimental protocols were approved by the animal ethic guidelines at experimental animal care, Suzhou University (Suzhou, China).

2.19. Rat TBI model

Six groups of rats were prepared as Sham group, TBI + Vehicle group, TBI + Rg1 (5 mg/kg) group, TBI + Rg1 (10 mg/kg) group, TBI + Rg1 (15 mg/kg) group and TBI + blebbistatin (10 mg/kg) group according to the instructions given previously[37]. Briefly, rats were subjected to anesthesia using 3.6% chloral hydrate (1 mL/100 g, ip) and underwent an incision of the skin overlying the scalp followed by the fixation of stainless-steel plate on the craniostosis with cement. Then, a 500 g weight was dropped from 100 cm through a guide tube onto the stainless-steel plate. After surgery, the scalp was sutured. Sham animals were subjected to the same procedures without injury. After injury for 30 min, Rg1 and blebbistatin were intraperitoneally injected into the corresponding rats. Rats were again administered with Rg1 or blebbistatin at 24 h after injury. Two days later, rats, serum and the brains were collected for analyses.

2.20. Evaluation of neurological outcome

According to the previous study[38], the neurological outcome was evaluated in terms of neurological severity score (NSS). The NSS comprised of 10 individual clinical parameters, including tasks on motor function, alertness and physiological behavior[39]. Higher score specified an inferior neurological outcome, and lesser score reflected a healthier neurological outcome assessed at 48 h after the surgery.

2.21. Measurement of brain water content

To examine the brain water content in rats using the dry and wet weight method[40], brain tissues were weighed on an electronic weighing balance before and after drying for more than 24 h at 60 °C overnight. Eq. (1) was used for brain water content (%) calculation:

$$\text{Brain water content}\,(\%) = (\text{Wet weight} - \text{Dry weight}) / \text{Wet weight} \times 100 \quad (1)$$

2.22. Evans blue assay

Evans blue extravasation was performed to investigate BBB permeability 48 h following TBI as described previously[40]. Briefly, Evans blue dye (2%; 4 mL/kg, Sigma−Aldrich) was infused for more than 2 min into blood circulation through the caudal vein. After 2 h, rats were anaesthetized, and brains were removed and observed. Then, removed brains were divided into left and right cerebral hemispheres for homogenate preparation. After centrifugation (at 15,000×*g* for 30 min), an equal volume of trichloroacetic acid was added to the resultant supernatant. The samples were again centrifuged at 15,000×*g* for 30 min after overnight incubation at 4 °C, and absorbance was measured at 615 nm by a spectrophotometer.

2.23. Immunofluorescence analysis

After cell fixation and permeabilization, they were incubated overnight with primary antibody at 4 °C followed by Alexa Fluor® 488 conjugated Donkey Anti-Goat IgG (H + L) antibody (Invitrogen, Carlsbad, CA, USA) and/or Alexa Fluor® 594 Donkey Anti-Goat IgG (H + L) antibody (Invitrogen, Carlsbad, CA, USA) and DAPI (Beyotime Biotechnology, China). The images were taken using a confocal microscope (Olympus, Tokyo, Japan).

2.24. Immunohistochemistry analysis

Brains were placed overnight in 4% paraformaldehyde (PFA) at pH 7.4, washed with PBS and then placed in graded sucrose solutions overnight before optimal cutting temperature compound (OCT, Sakura Finetek Japan, Tokyo, Japan) embedding[41]. Thick sections (5 μm) were cut and analyzed by immunostaining. Sections were stained with the immunohistochemistry kit (BOSTER Biological Technology Co. Ltd., Wuhan, China) following the manufacturer's instructions.

2.25. ELISA

IL-1β, TNF-α, and IL-6 contents were determined using commercial ELISA kits (Yifeixue Bio Tech, Nanjing, China) followed by measurement of optical density at 450 nm using Microplate Reader (M200 PRO, Tecan, Switzerland).

2.26. In situ hybridization

In situ hybridization was performed as described previously[14]. In brief, after hydration and antigen retrieval, 5-μm sections were incubated with double DIG (digoxigenin) labeled LNA probes (Exiqon, BOSTER Biological Technology Co. Ltd., China) overnight at 37 °C followed by SSC washes. An alkaline phosphatase-linked anti-DIG antibody (11093274910, Roche-Applied-Science, Mannheim, Germany) was used for visualization after which nitro blue tetrazolium chloride and 5-bromo-4-chloro-3-indolyl phosphate were administered (NBT-BCIP tablets, 11697471001, Roche-Applied-Science, Mannheim, Germany). DAPI was used as a nuclear counterstain. Slides were visualized using a confocal microscope (Olympus, Tokyo, Japan).

2.27. TUNEL staining

The sections (5 μm thick) were subjected to staining with TUNEL Bright Green apoptosis detection kit (Vazyme Biotech, Nanjing, China) following the manufacturer's instructions[42]. Slides were visualized using a confocal microscope (Olympus).

2.28. Statistical analysis

The obtained data was read as means ± standard error of mean (SEM). Student test or one-way analysis of variance (ANOVA) followed by Dunnett *post hoc* test were used to determine the significant difference at *P*-value of less than 0.05.

3. Results

3.1. Isolation and characterization of Exos

Macrophages are one of the sources of the exosomes. The THP-1 cells were induced by PMA (Fig. 1A). The results from the studies show that the pseudopods in the cell surface gradually outstretched leaving the space between. The cells gradually developed tentacles and moved towards the walls, indicating the differentiation into macrophages (Fig. 1A). The structure, size and number of the isolated Exos were identified by TEM and NanoSight particle tracking analysis (Fig. 1B and C). The macrophage-derived Exos were cup-shaped with the size range of about 100 nm. A slightly high yield of IIM-Exos was obtained from IL-1β-induced macrophages group as compared to the NM-Exos group. In addition, typical Exos markers CD63 and CD9 were perceived by Western blot (Fig. 1D and E). The significant finding of CD63 and CD9 in IIM-Exos group as compared to the NM-Exos group indicated the successful isolation of Exos.

3.2. Rg1 improved HBMECs injury via inhibiting macrophage-derived Exos miR-21

Clinical and experimental studies have shown that secreted miR-21 plays a key role in cranio-cerebral injury[14]. Therefore, TaqMan-based quantitative real-time PCR analysis was used to detect the expression of miR-21-5p in different processing macrophage-derived Exos groups. The results confirm that the expression of miR-21-5p was higher in IIM-Exos, whereas the expression level of miR-21-5p was declined after Rg1 or blebbistatin or MYH9-siRNA (NMIIA inhibitor blebbistatin or NMIIA gene MYH9 interference) treatment in macrophages (Fig. 2A−C). The reduced expression illustrated that inhibition of NMIIA could significantly inhibit the macrophage-derived Exos miR-21. The inhibition of macrophage-derived Exos miR-21 release by Rg1 may pass through NMIIA. Furthermore, internalization of macrophage-derived Exos in HBMECs were visualized by PKH67 fluorescent tracer technique. PKH67 labeled macrophage-derived Exos was remarkably localized in HBMECs after co-culture for 18 h (Fig. 2D). In addition, the expression levels of MMP-1, -3, and -9 in HBMECs were assessed by Western blot and quantification analysis. Results show that the expression of MMP-1, MMP-3 and MMP-9 in the IIM-Exos stimulation group was significantly higher than that in the NM-Exos group ($P < 0.01$). In contrast, the expression of MMP-1,

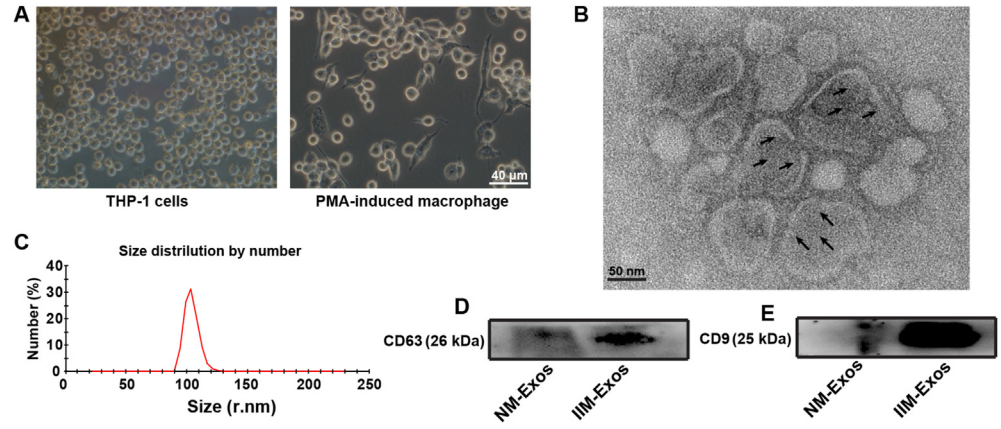

Figure 1 Isolation and characterization of IL-1β-induced macrophages Exos. (A) The THP-1 cells were induced to macrophages by PMA (100 ng/mL). Scale bar 40 μm. (B) Ultrastructure of macrophage-derived Exos (IIM-Exos) was observed by TEM. The representative electron microscopy image shows somehow circular membrane-bound vesicles (100 nm). Scale bar 50 nm. (C) NanoSight particle tracking analysis displaying different sizes of Exos. The value of the abscissa represents the mean particle size within each nanometer thickness range. (D) Standard markers CD63 and CD9 were detected by Western blot in macrophage-derived Exos.

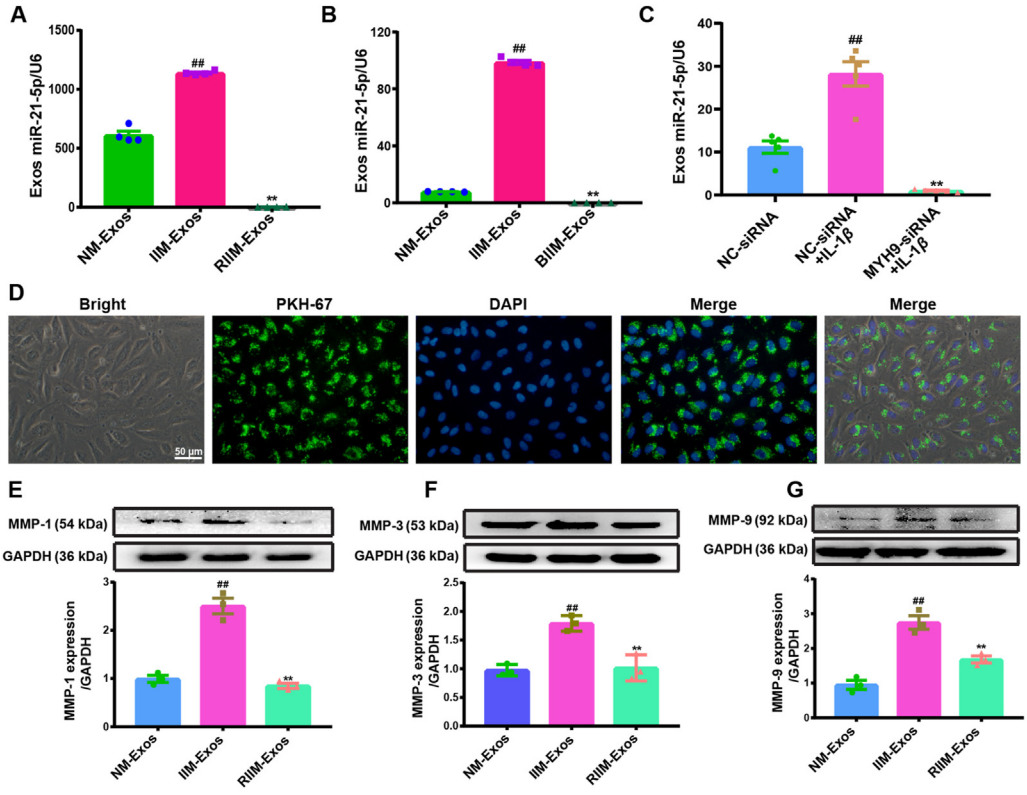

Figure 2 Rg1 improves HBMECs injury *via* inhibiting macrophage-derived Exos miR-21. (A)−(C) TaqMan-based quantitative real-time PCR analysis of miR-21-5p expression in macrophage-derived Exos. (D) Confocal microscopy analysis of PKH67-labeled macrophage-derived Exos localized in HBMECs. Representative micrographs of PKH67-labeled Exos in HBMECs are in merge images. The Exos-labeled PKH67 in HBMECs shows green fluorescence. Nuclei were counterstained with DAPI (blue fluorescence). Scale bar 50 μm. (E) The expressions of MMP-1, MMP-3, and MMP-9 were assessed by Western blot and quantification analysis. Data represent mean ± SEM of three or more independent experiments. $^{\#}P < 0.05$, $^{\#\#}P < 0.01$ *vs.* NM-Exos group; $^{*}P < 0.05$, $^{**}P < 0.01$ *vs.* IIM-Exos group.

MMP-3 and MMP-9 in the RIIM-Exos group was significantly lower than that in the IIM-Exos group ($P < 0.01$) (Fig. 2E−G). Acquisitively, these findings indicate that Rg1 inhibited matrix metalloproteinases-1, -3 and -9 expression and ameliorated the HBMECs injury.

3.3. Rg1 improves BBB permeation via inhibiting macrophage-derived Exos miR-21

Fig. 3A−C reveals that treatment of HBMECs with IIM-Exos miR-21 downregulated the levels of ZO-1, occludin and claudin-

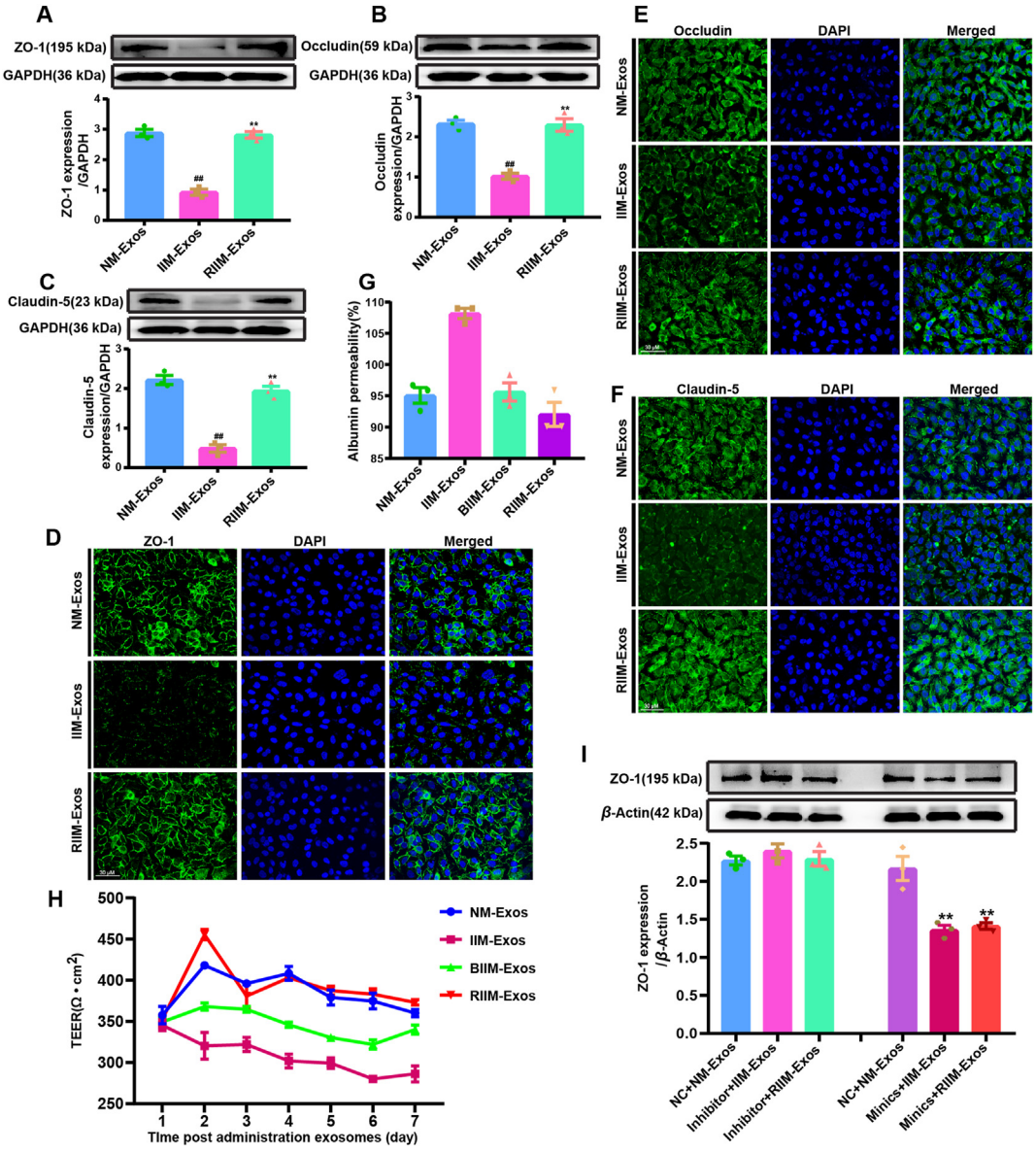

Figure 3 Rg1 improves blood−brain barrier permeation *via* inhibiting macrophage-derived Exos miR-21. (A)−(C) The expressions of tight junction proteins in HBMECs. (D)−(F) The expressions of tight junction protein in HBMECs were detected by immunofluorescence. (G) Blood−brain barrier function was validated by analysis of Evens blue (EB) albumin leakage assays. (H) Trans endothelial electric resistance (TEER) was used to detect the permeability of BBB. (I) After 24 h of the HBMECs treatment with negative control (80 nmol/L), miR-21-5p inhibitor (80 nmol/L) and minics (80 nmol/L), combined NM-EVs (100 μg/mL), IIM-EVs (100 μg/mL) and RIIM-EVs (100 μg/mL). Data represent mean ± SEM of three or more independent experiments. $^{\#}P < 0.05$, $^{\#\#}P < 0.01$ *vs.* NM-Exos; $^{*}P < 0.05$, $^{**}P < 0.01$ *vs.* IIM-Exos.

5 ($P < 0.01$), while RIIM-Exos miR-21 pre-treatment significantly promoted the up-regulations of ZO-1, occludin and claudin-5 ($P < 0.01$). Similarly, immunofluorescence staining analysis also confirmed that IIM-Exos miR-21 significantly promoted the degradation of TJPs (ZO-1, occludin and claudin-5), while RIIM-Exos pre-treatment significantly blocked the degradation of TJPs (Fig. 3D−F). As tight junction proteins are important components of the BBB, a further confirmation of BBB function was validated by analysis of Evans blue permeation and trans-endothelial electrical resistance (TEER). As seen in Fig. 3G, the integrity of HBMECs monolayer was gradually increased with lower Evans blue albumin permeability following by NM-Exos stimulation. Compared with NM-Exos, IL-1β-induced macrophage-derived Exos miR-21 (IIM-Exos) significantly increased Evans blue albumin permeability. IL-1β-induced macrophage-derived Exos miR-21 with Rg1 or blebbistatin pre-treatment (*i.e.*, RIIM-Exos or BIIM-Exos) significantly decreased the Evans blue albumin permeability, suggesting that Rg1 or blebbistatin improved the permeability of BBB. Consistent with these results, IIM-Exos miR-21 significantly decreased TEER, suggesting that IIM-Exos miR-21 damaged the BBB integrity (Fig. 3H). RIIM-Exos or BIIM-Exos pre-treatment significantly increased TEER, suggesting that Rg1 or blebbistatin protected the BBB integrity (Fig. 3H). In addition, miR-21-5p inhibitor and minic were used to determine whether miR-21-5p was involved in the effects of Exos on HBMECs ZO-1 expression. The inhibitory effect of IIM-Exos on

the ZO-1 expression of HBMECs was reversed by the miR-21-5p inhibitor. The promoting effects of RIIM-Exos on the ZO-1 expression of HBMECs were canceled by the miR-21-5p mimics (Fig. 3I). These results suggest that miR-21-5p in Exos could inhibit the HBMECs ZO-1 expression.

3.4. Exos miR-21 directly targeted the TIMP3 and affects NF-κB signaling pathway in HBMECs

As per the TargetScanHuman (http://www.targetscan.org/), tissue inhibitor of matrix metalloproteinases (TIMP3), a protein interceding cellular glycosylation[4], may be a target of miR-21-5p. The projected site of the combination was situated at 1032−1039 of TIMP3 3′-UTR (Fig. 4A). Luciferase activity was pointedly repressed after co-transfection with pre-miR-21-5p in wild-type and mutant 293T cells. The pre-miR-21-5p inhibitory activity of luciferase in mutant 293T cells decreased significantly compared with wild-type 293T cells ($P < 0.01$), demonstrating that TIMP3 was a target of miR-21-5p (Fig. 4B). Thus, the effects of Exos miR-21-5p on TIMP3 mRNA and protein expression in HBMECs were evaluated. High miR-21-5p in IIM-Exos dramatically inhibited TIMP3 mRNA and protein expression in HBMECs. Lower levels of miR-21-5p in both RIIM-Exos and BIIM-Exos significantly upregulated the TIMP3 mRNA and protein expression in HBMECs compared with IIM-Exos group (Fig. 4C and D). Consistent with these results, inhibitor and minics of miR-21-5p were used to determine the role of miR-21-5p in the effects of Exos on TIMP3 expression in HBMECs. The inhibitory effect of IIM-Exos miR-21-5p on the TIMP3 expression in HBMECs was reversed by the miR-21-5p inhibitor. The endorsing effects of RIIM-Exos miR-21-5p on the TIMP3 expression in HBMECs were canceled by the miR-21-5p minics (Fig. 4E). Furthermore, miR-21-5p expression or TIMP3 suppression likewise encouraged the NF-κB phosphorylation (Fig. 4F), while TIMP3 overexpression repressed the NF-κB phosphorylation. These results provide the evidence that miR-21-5p could inhibit the TIMP3 expression in HBMECs. IIM-Exos transferring an army of miR-21-5p inhibited the TIMP3 expression, while, RIIM-Exos carrying a small amount of miR-21-5p promoted the TIMP3 expression. MiR-21-5p influenced the

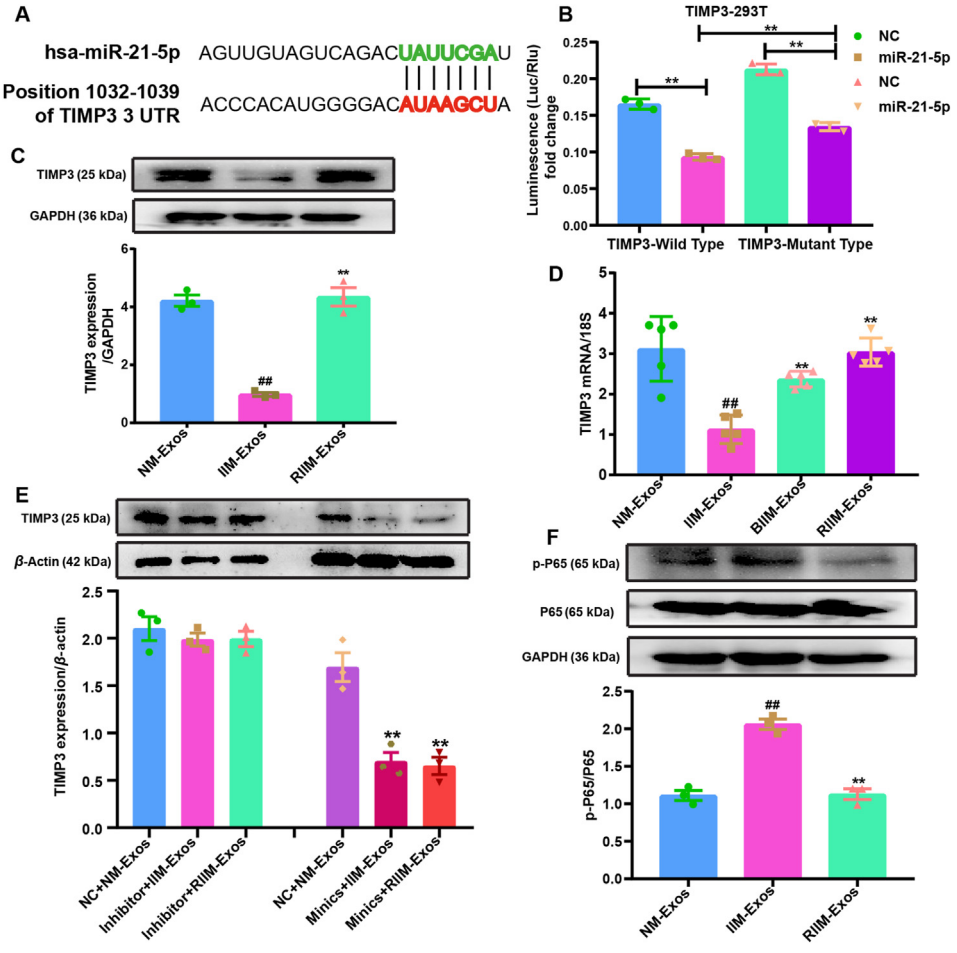

Figure 4 TIMP3 as a direct downstream target of Exos miR-21-5p in HBMECs activation. (A) Projected site of the hsa-miR-21-5p mixture. (B) TIMP3 as a target of hsa-miR-21-5p in 293 T cells. (C) and (D) Effects of miR-21-5p from NM-Exos, IIM-Exos, RIIM-Exos, and BIIM-Exos on TIMP3 mRNA and protein expressions in HBMECs. After 24 h of transferring NM-Exos (100 μg/mL), IIM-Exos (100 μg/mL), RIIM-Exos (100 μg/mL) and BIIM-Exos (100 μg/mL) to the media of HBMECs. (E) After 24 h of HBMECs treatment with negative control (NC, 80 nmol/L), miR-21-5p inhibitor (80 nmol/L) and miR-21-5p minics (80 nmol/L), combined with NM-Exos (100 μg/mL), IIM-Exos (100 μg/mL) or RIIM-Exos (100 μg/mL). (F) NF-κB P65 and phosphorylated P65 expression. Data represent mean ± SEM of three or more independent experiments. $^{\#}P < 0.05$, $^{\#\#}P < 0.01$ *vs.* NM-Exos; $^{*}P < 0.05$, $^{**}P < 0.01$ *vs.* IIM-Exos.

HBMECs function by interceding the activation of NF-κB signaling.

3.5. *Interfering the interactions of NMIIA−HSP90 by Rg1 controls exosome release in macrophages*

Because non-muscle myosin IIA (NMIIA) is an actin-based motor protein[28,29] essential to the stepwise cytoskeletal reorganization[7] and lytic granule release[8]. We sought to test whether NMIIA controls extracellular secretion or not. Upon IL-1β stimulation of PMA-induced macrophages that express endogenous NMIIA protein, it was found that the Exos-associated protein TSG101 evacuated from the cell cytosol, indicating that abundant Exos contained NMIIA were released from the cytoplasm to the extracellular (Fig. 5A). Consistent with these results, we then further co-localized NMIIA with TSG101 in PMA-induced macrophages that constitutively secrete Exos. It was observed that TSG101 was with a discrete vesicular-like distribution, while, NMIIA was more evenly expressed across the cytosol, clearly distinguishing NMIIA from a canonical vesicular protein (Fig. 5B and C). Fig. 5A−C collectively show that Rg1 or blebbistatin pretreatment significantly reduced the macrophage-derived Exos release. Furthermore, to investigate the interactions of NMIIA in the regulation of Exos release, NMIIA antibody was then used for co-immunoprecipitation (Fig. 5D). The amount of ~230 and ~90 kD proteins, as found by SDS-PAGE, progressively increased in macrophages followed by IL-1β stimulation. MALDI-TOF-MS analyses of the ~230 and ~90 kD proteins identified them as NMIIA and HSP90 (Supporting Information Fig. S1), suggesting that HSP90 might be a specific binding protein of NMIIA. Similar results were seen after performing the co-immunoprecipitation assay (Fig. 5E) and Western blot (Fig. 5A). These results demonstrate that interfering the interactions of NMIIA−HSP90 by Rg1 altered the subcellular localization, where diffused cytoplasmic distribution associates to extracellular discharge.

3.6. *Rg1 administration decreased the BBB permeability and inflammation early following traumatic brain injury (TBI)*

With an aim to reveal the severity level of brain injury in different experimental groups, we assessed the thoroughness of nerve injury, brain water content and Evans blue infiltration examination of brain tissues. It was found that severity score of nerve injury in TBI group was developed in comparison to Sham group (Fig. 6A), brain water content (Fig. 6B), and Evans blue osmotic volume (Fig. 6C and D). A pretreatment with Rg1 or blebbistatin after TBI

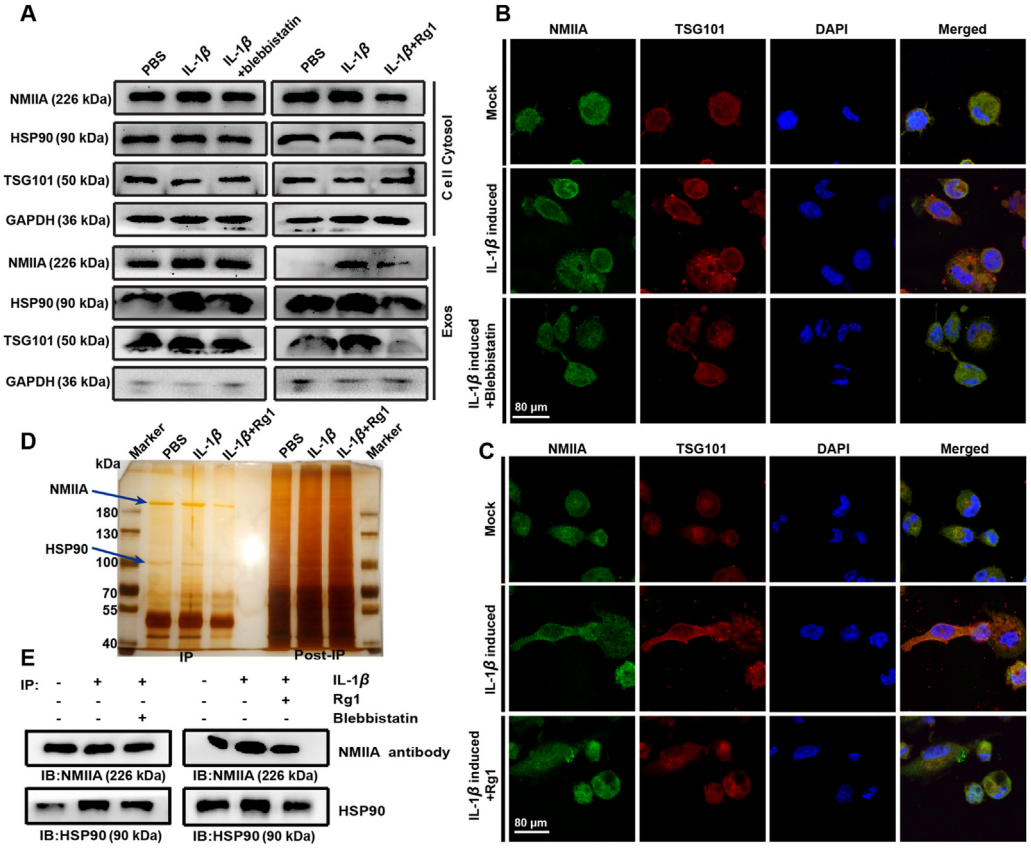

Figure 5 Interfering the interactions of NMIIA-HSP90 by Rg1 controls exosome release. (A) PMA-induced macrophages were treated with IL-1β (20 ng/mL) with or without Rg1 and blebbistatin (1 μmol/L) for the indicated time. Then, Exos in the supernatant and cell cytosols were collected respectively later. NMIIA, HSP90, TSG101 and GAPDH expression were detected by Western blot. (B)−(C) Immunofluorescence co-localization of NMIIA (green signal) with the exosome marker TSG101 (red signal) using confocal immunofluorescence. Representative micrographs were revealed. Scale bars represent 80 μm. (D) NMIIA and HSP90 were identified by co-immunoprecipitation combined with MALDI-TOF-MS assays in PMA-induced macrophages. (E) Macrophages were immunoprecipitated with NMIIA antibody and these complexes were separated by SDS-PAGE followed by immunoblotting analysis.

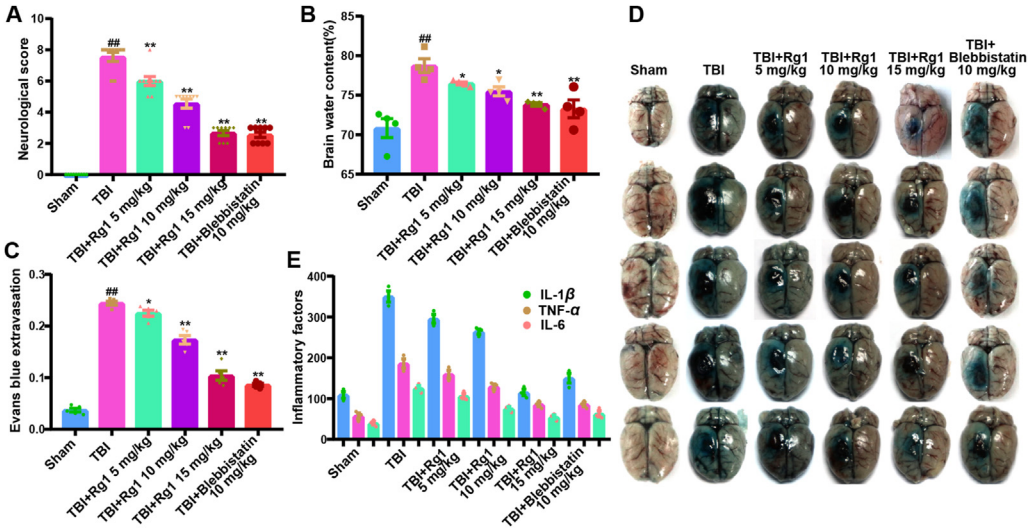

Figure 6 Rg1 administration decreased the BBB permeability and inflammation early following TBI. (A) Nerve injury severity score (NSS) of all the experimental groups. (B) Brain tissue water content was used to determine the weight of dry-wet assay. (C) Quantification of Evans blue content in the brain. (D) Images showing Evans blue extravasation in Sham, TBI + vehicle, TBI + Rg1, and TBI + blebbistatin groups on the 2nd day after TBI. (E) Serum inflammatory cytokines (IL-1β, TNF-α, and IL-6) were measured by ELISA. Data represent mean ± SEM of three or more independent experiments. $^{\#}P < 0.05$, $^{\#\#}P < 0.01$ *vs.* Sham group; $^{*}P < 0.05$, $^{**}P < 0.01$ *vs.* TBI group.

showed significantly lower disease severity score as compared to non-treatment group. Interestingly, the significant difference was increased on gradual increase of dose of Rg1 or blebbistatin indicating a dose-dependent relationship against TBI and Rg1 or blebbistatin (Fig. 6A–D). These results indicate that Rg1 or blebbistatin pretreatment had a significant inhibitory effect on BBB permeability and protective effects against TBI injury. Moreover, the serum levels of inflammatory cytokines including IL-1β, TNF-α, and IL-6 drastically increased in response to TBI; alternatively, our results show that Rg1 or blebbistatin

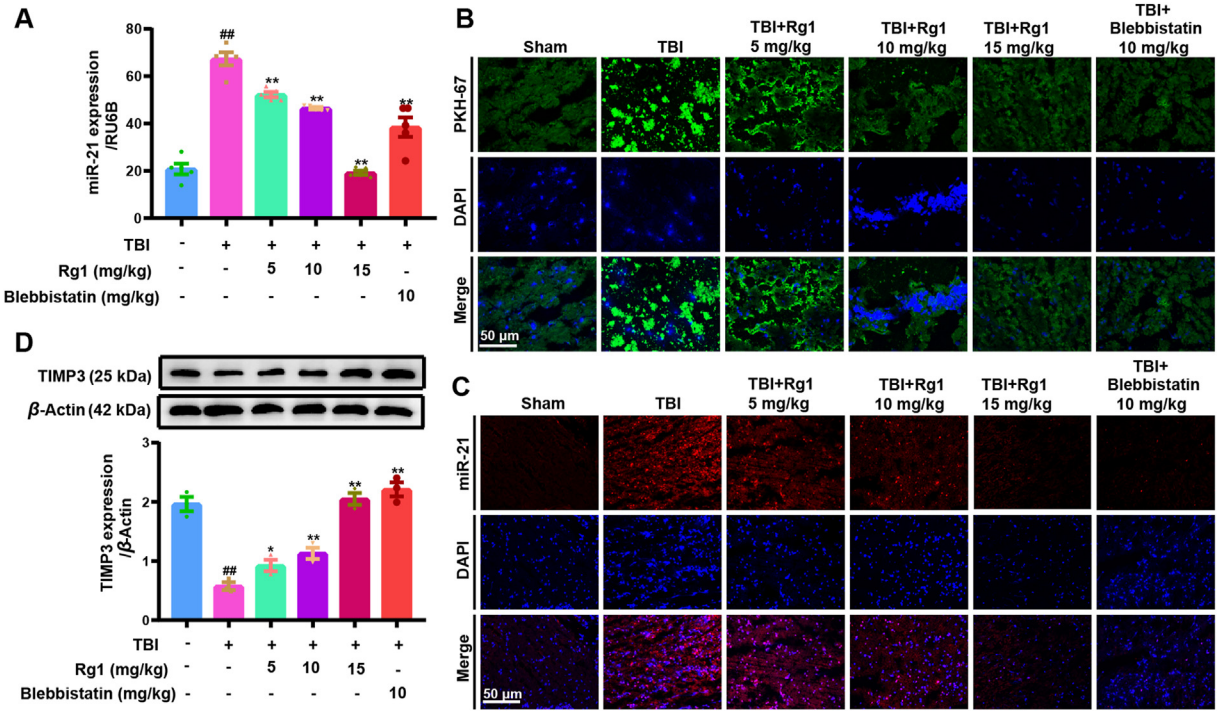

Figure 7 Rg1 inhibits the release of Exos miR-21 in peripheral blood transferring to the brain. (A) Exos miR-21-5p expression in serum in peripheral blood. (B) The number of secretory micro-vesicles in brain tissue was labeled with PKH67 fluorescent dye. (C) The content of miR-21 in brain tissue was evaluated by *in situ* hybridization of miR-21-5p (red) with TBI lesions from the mice. Scale bars 50 μm. (D) TIMP3 expression in brain tissue. Data represent mean ± SEM of three or more independent experiments. $^{\#}P < 0.05$, $^{\#\#}P < 0.01$ *vs.* Sham group; $^{*}P < 0.05$, $^{**}P < 0.01$ *vs.* TBI group.

administration to rats significantly decreased the IL-1β, TNF-α, and IL-6 levels in serum compared with TBI (Fig. 6E).

3.7. *Rg1 inhibited the release of Exos miR-21 in peripheral blood transferring to the brain*

After experimental TBI, we isolated serum Exos and further examined the expression of Exos miR-21 in peripheral blood. It was found that Exos miR-21 levels in serum remarkably improved after TBI, and reduced after Rg1 treatment (Fig. 7A). Using PKH67 fluorescence tracer technique, Exos (green) levels in brain tissue sections in TBI group was significantly increased (Fig. 7B) alternatively, Rg1 dose-dependently restricted the uplift of Exos (green) level in brain tissue sections, indicating that Rg1 can inhibit Exos from peripheral blood flow towards the brain. Furthermore, FISH assay showed that Exos miR-21 (red) in TBI group was significantly improved (Fig. 7C), and Rg1 significantly subdued the Exos miR-21 levels in brain tissue, indicating that Rg1 may inhibit Exos miR-21 levels in brain tissue. Consistent with the functions of Rg1, blebbistatin treatment also functionally decreased the release of Exos miR-21 in peripheral blood which was further supposed to flow towards brain (Fig. 7A–C). To assess the target of miR-21 from peripheral blood in brain tissue, TIMP3 expression was measured using Western blot analysis. Fig. 7D reveals that TIMP3 was markedly reduced after injury while a pretreatment with Rg1 or blebbistatin restricted this variation. Altogether, these data suggest that Rg1 inhibited the release of Exos miR-21 in peripheral blood flow towards brain and blocked the degradation of TIMP3 *in vivo*.

3.8. *Rg1 protected from BBB damage by inhibiting MMPs expressions against deprivation of tight junction proteins in rats*

In order to further confirm that Exos wrapped miR-21 served as a regulatory factor in brain tissue and could interfere with the degradation of TJPs, the expression levels of ZO-1 (Fig. 8A), occludin (Fig. 8B) and claudin-5 (Fig. 8C) in brain tissues were assessed. The outcomes showed that the TJPs (ZO-1, occludin and claudin-5) expression levels were decreased swiftly after craniocerebral injury, while the expressions of TJPs were dose-dependently upregulated after treatment with Rg1 or blebbistatin. Further detection of ZO-1 in brain tissue sections by

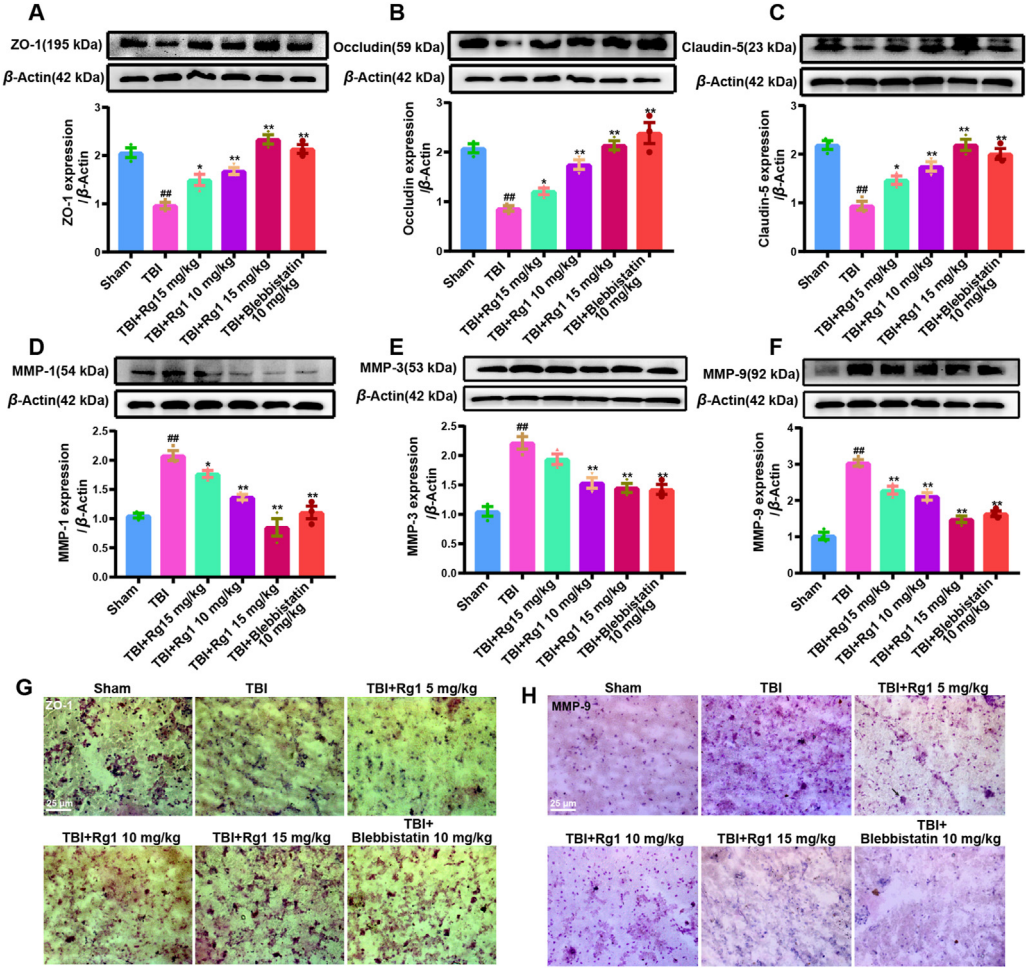

Figure 8 Rg1 protected BBB damage by inhibiting MMPs expressions against degradation of TJPs in rats. (A)–(C) The TJPs expression levels in brain tissues were analyzed by Western blot. (D)–(F) Expression levels of MMP-1, MMP-3, and MMP-9 protein in brain tissue. (G) Immunohistochemical technique was used to evaluate the expression of ZO-1 protein (brown granules) in brain tissues. Scale bars 25 μm. (H) The expression level of MMP-9 protein (purple granules) in brain tissues was evaluated by immunohistochemical technique. Scale bars 25 μm. Data represent mean ± SEM of three or more independent experiments. $^{\#}P < 0.05$, $^{\#\#}P < 0.01$ *vs.* Sham group; $^{*}P < 0.05$, $^{**}P < 0.01$ *vs.* TBI group.

immunohistochemical technique, showed a decrement of ZO-1 in TBI group (expression level of brown granule; Fig. 7G). It was found that content of ZO-1 improved after treatment with Rg1 or blebbistatin, indirectly indicated that Rg1 or blebbistatin suppressed the degradation of TJPs in brain tissue after TBI. Upon the analyses of MMPs, Western blot assay presented that the expression levels of matrix protease MMP-1 (Fig. 8D), MMP-3 (Fig. 8E) and MMP-9 (Fig. 8F) in TBI group were increased significantly ($P < 0.01$), and dose-dependently decreased with Rg1 or blebbistatin treatment. Similarly, the results of immunohistochemistry analyses confirmed that the content of MMP-9 in brain tissue of TBI group was higher than that in Sham group, and it was significantly decreased after Rg1 or blebbistatin administration. Altogether, these data demonstrate that Rg1 served as protective shield for TJPs in rats by playing its potential inhibitory role against MMPs.

3.9. Rg1 may reduce apoptosis and secrete VEGF to improve the neural functional in rats

The vascular endothelial growth factor (VEGF) acts as an effective proangiogenic factor[43]. The lowered cerebral VEGF/VEGF-A levels in mice were linked to reduced blood vessel density, lower neural structure density, reduced synapses, and decreased neurogenesis[44]. In this study, Western blot and immunohistochemistry methods were firstly used to evaluate the glial fibrillary acidic protein (GFAP) expression in brain tissues (Fig. 9A and B). The results exhibit that the content of GFAP protein in TBI group was lowered, and the expression of GFAP protein was significantly upregulated after Rg1 or blebbistatin treatment, indicating that Rg1 or blebbistatin had protective effect on neuroproteins. In order to approve the anti-apoptosis effect of Rg1, the expression level of VEGF in brain tissues was analyzed (Fig. 9C). Our findings specified that the content of VEGF protein in TBI group was lesser, and the protein expression of VEGF after Rg1 or blebbistatin administration was remarkably upregulated, suggesting that the increased VEGF by Rg1 improved nerve function. Upon TUNEL staining, significant apoptosis effects (green color granules) were observed in TBI group (Fig. 9D). Interestingly, Rg1 or blebbistatin treatment after the injury showed swift downregulation of apoptosis, indicating their potential contributory role in neuronal repair against the injury. In addition, we further investigated the anti-apoptotic signaling pathway of Rg1. The results show that Rg1 or blebbistatin administration dramatically attenuated TBI induced NF-κB activation (Fig. 9E).

4. Discussion

Following the traumatic brain injury (the primary, mechanical injury), secondary brain damageis accompanied by various biomolecular and pathophysiological responses[1,11,15,37]. Since these secondary events occur after the trauma and may appear within few hours to days, fair chances can be availed for therapeutic targeting to prevent further deterioration. Lately, miRNAs are recognized as relevant posttranscriptional regulators of various cellular functions in the brain[15,45]. The remarkable upregulation was observed in Exos miR-21 of serum after TBI, while the treatment with ginsenoside Rg1 resulted into a significant decrease in the expression level of Exos miR-21. Ginsenoside Rg1 inhibited the release of Exos miR-21 in peripheral blood flow to the brain leading to a new mechanism of action for Rg1. Our findings from the present study and earlier reported results[11,14,15] further

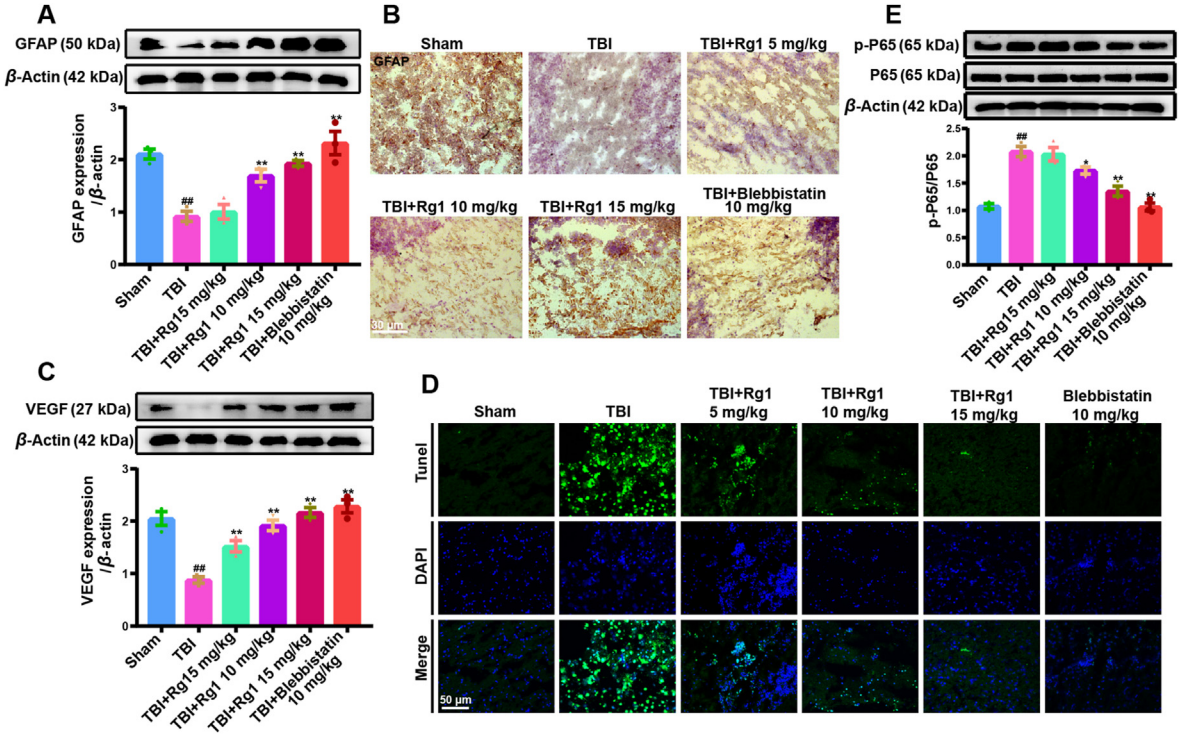

Figure 9 Rg1 may reduce apoptosis and secrete VEGF to improve neural functional in rats. (A), (C), (E) Analysis of GFAP, VEGF, p-P65 and P65 protein expression in brain tissues. (B) Analysis of GFAP protein expression (brown neurons) in brain tissues was observed by immunohistochemistry. Scale bars 25 μm. (D) TUNEL detection and evaluation of the level of brain neuronal apoptosis. Scale bars 50 μm. Data represent mean ± SEM of three or moreindependent experiments. $^{\#}P < 0.05$, $^{\#\#}P < 0.01$ *vs.* Sham group; $^{*}P < 0.05$, $^{**}P < 0.01$ *vs.* TBI group.

suggested that miR-21 is an important functional molecule, which acts as a biomarker for diagnosis and treatment in TBI.

BBB regulates ionbalance, nutrient transport and blocks the possibly detrimental particles that act as an interface between the CNS and peripheral circulatory system[46,47]; and it consists of specific brain capillary endothelial cells for highly specialized transport system[48,49]. Disruption of BBB and TJPs strictly disturb the neuronal functions and lead to neurological diseases[46]. Herein, we observed that ginsenoside Rg1 could significantly improve the neurological deficits, brain edema, BBB permeability, inflammatory factors, and related protein levels in the TBI, indicating that natural active ginsenoside Rg1 is a good protective agent of BBB. Besides digesting TJPs and indicating their key roles in BBB disruption, matrix metalloproteinases (MMPs) minerals dependent enzymes modulate many intercellular signaling mechanisms[4,50]. The present study revealed that high expression of MMPs including MMP-1, -3, and -9 in HBMECs could strongly promote the degradation of TJPs and damage the BBB in TBI. Ginsenoside Rg1 protected the integrity of the BBB in TBI by increasing TIMP3 protein expression and accelerated MMPs proteolysis. The controlled proteolytic activity of MMPs played an imperative part in development and maintenance of CNS.

MiR-21 is negatively associated to the BBB in TBI and participates in the disruption of tight junctions[11,14,51]. The low level of miR-21-5p played beneficial roles in attenuating BBB permeability, neuroinflammation, brain edema, and neurological deficits in TBI rats, suggesting that reducing miR-21-5p may serve as a possible therapeutic approach in the treatment of TBI. It was interesting that the change of exosome miR-21-3p was not very significant (data not shown), which is not consistent with previous report[52]. The reason for this difference may be due to the fact that miR-21 originate from exosomes. Bioinformatic analysis and dual luciferase assay exhibited TIMP3 as an essential target of miR-21-5p, which was further experimentally established from our results indicating that miR-21-5p subdued TIMP3 mRNA and protein expressions in HBMECs and in brain tissues of TBI. Alternatively, IIM-Exos inhibited TIMP expressions and increased miR-21-5p levels in HBMECs and in brain tissues of TBI. Our results indicate that miR-21-5p accelerated HBMECs damage *via* lowering the TIMP expression. The neuroprotective action of RIIM-Exos was facilitated by the inhibitory effect of miR-21-5p on TIMP expressions in HBMECs.

While exploring the natural products, ginsenoside Rg1 is an important chemical constituent from ginseng responsible for the neurotrophic and neuroprotective effects in CNS. Although other isoforms of non-muscles myosin, particularly NMIIC have been reported to link with brain injury, however the association of NMIIA has been profoundly found connected with TBI[53]. Earlier studies have reported that Rg1 was associated with the regulation of NMIIA-actin cytoskeletal structure in certain neurological diseases[54,55]. In this study, our results show that inhibition of NMIIA by Rg1 may significantly restrain macrophage-derived Exos miR-21 release. Co-immunoprecipitation and MALDI-TOF-MS assays show that HSP90 was one of the interactors of NMIIA in macrophages. Therefore, prying the interactions of NMIIA−HSP90 by Rg1 or blebbistatin can effectively control exosome release. Our results show that ginsenoside Rg1 can suppress the secretion of exosome-miR-21 transferred to the brain *via* inhibiting the interaction of NMIIA and HSP90 in macrophages. These findings further spot a niche for future studies signifying that an interference in protein−protein interactions by natural products might be considered as a new strategy for

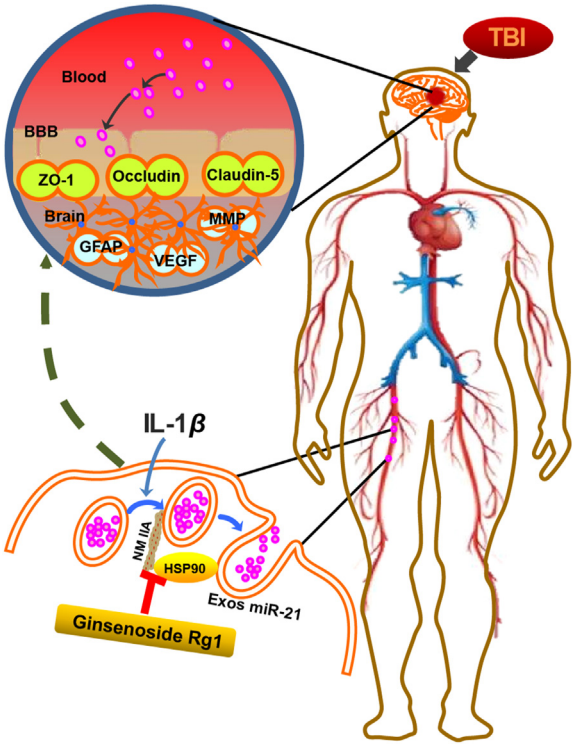

Figure 10 Proposed signaling mechanism of ginsenoside Rg1 from ginseng for the therapeutic utility *via* multiple directions converging to one objective of traumatic brain injury treatment. BBB, blood−brain barrier; HSP, heat shock protein: NMIIA, non muscle myosin IIA; Exos-miR-21, exosomal micro RNA-21; IL-1β, interlukin 1-β; ZO-1, zona occuludin-1; VEGF, vesicular endothelial growth factor; MMP, matrix metallo proteinases.

mediating extracellular vesicles release. However, the exact mechanism of interaction between particular functional domain of NMIIA with Rg1 and HSP90 is still not confirmed and may require *Myh9*$^{-/-}$ and *Hsp90*$^{-/-}$ experimental animals for *in vivo* confirmation.

Neuroinflammation exerts a negative effect on brain cells and also plays a role in brain edema[56]. We evaluated the release of exosome miR-21 transferring to the injured brain from peripheral blood after TBI. The exosomal miR-21 flow to BBB activates the NF-κB signaling pathway that consequently leads to neuronal inflammation. In return, this inflammation inhibits the VEGF expression and consequently induces the nerve apoptosis and leads to damaged GFAP proteins. Interestingly, our results show that ginsenoside Rg1 can inhibit the exosomal miR-21 release in peripheral blood thus improving the neuroinflammation by less BBB permeability and ultimately reducing the nerve apoptosis in response to TBI. It is necessary that peripheral blood exosomes miR-21 crossing the BBB dynamically in the model of TBI are visualized by real-time dynamic monitoring, which will be further studied in the future.

5. Conclusions

The data presented in this study suggest that ginsenoside Rg1 may improve the effects of cerebral vascular endothelial injury, protect the integrity of the BBB, and has a considerable potential for the

treatment of TBI. It was further concluded that ginsenoside Rg1 could suppress the secretion of exosome-miR-21 transferred to the brain by restricting the interaction of NMIIA and HSP90 in macrophages. Our findings implicated the novel mechanism of ginsenoside Rg1 in the management of TBI disease, revealing the biological signal transduction characteristics and signaling pathways of exosomal miR-21 cross-cerebral microvascular endothelial cells (Fig. 10). Targeting the interactive triad of NMIIA−HSP90−ginsenoside Rg1 provides a new research direction for the prevention and treatment of cerebrovascular disease.

Acknowledgments

This work was supported by National Natural Science Foundation of China (81601034 and 31850410476), Anhui Provincial Science Fund for Distinguished Young Scholars (2008085J39, China), Focus on Research and Development Projects in Anhui Province (1804a0802225, China), State Key Laboratory for Chemistry and Molecular Engineering of Medicinal Resources (CMEMR2020-B13, Guangxi Normal University, China), the Natural Science Foundation of Anhui Educational Committee (KJ2018ZD044 and KJ2020A0728, China), Key Disciplines of Pharmacy (2019xjzdxk2, China), the Back-up Candidates for Academic and Technical Leaders of Suzhou University (2018XJHB06, China), and Key Research Project of Suzhou University (2019yzd06, China).

Author contributions

Kefeng Zhai, Wei Wang, and Siyu Zhao designed and performed biological experimentation and figured out the findings. Yuhan Zhang and Ghulam Jilany Khan performed and analyzed *in vivo* experiments. Kiran Thakur and Xuemei Fang wrote the manuscript and designed/arranged the data for manuscript writing. Mengting Wang and Chao Wu contributed to *in vivo* experiments and general experimental design and corrected the manuscript. Hong Duan and Jianbo Xiao supervised the studies and guided for the experimentation theme of the study. Zhaojun Wei arranged the data for manuscript publication and corresponded for the publication.

Conflicts of interest

The authors declare that there are no conflicts of interest.

Appendix A. Supporting information

Supporting data to this article can be found online at https://doi.org/10.1016/j.apsb.2021.03.032.

References

1. Liu YL, Xu ZM, Yang GY, Yang DX, Ding J, Chen H, et al. Sesamin alleviates blood−brain barrier disruption in mice with experimental traumatic brain injury. *Acta Pharmacol Sin* 2017;**38**:1445−55.
2. Zhu B, Eom J, Hunt RF. Transplanted interneurons improve memory precision after traumatic brain injury. *Nat Commun* 2019;**10**:5156.
3. Kaur P, Sharma S. Recent advances in pathophysiology of traumatic brain injury. *Curr Neuropharmacol* 2018;**16**:1224−38.
4. Dhanda S, Sandhir R. Blood−brain barrier permeability is exacerbated in experimental model of hepatic encephalopathy *via* MMP-9 activation and downregulation of tight junction proteins. *Mol Neurobiol* 2018;**55**:3642−59.
5. Ha D, Yang N, Nadithe V. Exosomes as therapeutic drug carriers and delivery vehicles across biological membranes: current perspectives and future challenges. *Acta Pharm Sin B* 2016;**6**:287−96.
6. Song L, Tang S, Han X, Jiang Z, Dong L, Liu C, et al. KIBRA controls exosome secretion *via* inhibiting the proteasomal degradation of Rab27a. *Nat Commun* 2019;**10**:1639.
7. Iizuka Y, Cichocki F, Sieben A, Sforza F, Karim R, Coughlin K, et al. UNC-45A is a nonmuscle myosin IIA chaperone required for NK cell cytotoxicity *via* control of lytic granule secretion. *J Immunol* 2015;**195**:4760−70.
8. Li P, Wei G, Cao Y, Deng Q, Han X, Huang X, et al. Myosin IIa is critical for cAMP-mediated endothelial secretion of von Willebrand factor. *Blood* 2018;**131**:686−98.
9. Van Niel G, d'Angelo G, Raposo G. Shedding light on the cell biology of extracellular vesicles. *Nat Rev Mol Cell Biol* 2018;**19**:213−28.
10. Osier N, Motamedi V, Edwards K, Puccio A, Diaz-Arrastia R, Kenney K, et al. Exosomes in acquired neurological disorders: new insights into pathophysiology and treatment. *Mol Neurobiol* 2018;**55**:9280−93.
11. Di Pietro V, Ragusa M, Davies D, Su Z, Hazeldine J, Lazzarino G, et al. MicroRNAs as novel biomarkers for the diagnosis and prognosis of mild and severe traumatic brain injury. *J Neurotrauma* 2017;**34**:1948−56.
12. Hartmann D, Fiedler J, Sonnenschein K, Just A, Pfanne A, Zimmer K, et al. MicroRNA-based therapy of GATA2-deficient vascular disease. *Circulation* 2016;**134**:1973−90.
13. Li X, Tian Y, Tu MJ, Ho PY, Batra N, Yu AM. Bioengineered miR-27b-3p and miR-328-3p modulate drug metabolism and disposition *via* the regulation of target ADME gene expression. *Acta Pharm Sin B* 2019;**9**:639−47.
14. Harrison EB, Hochfelder CG, Lamberty BG, Meays BM, Morsey BM, Kelso ML, et al. Traumatic brain injury increases levels of miR-21 in extracellular vesicles: implications for neuroinflammation. *FEBS Open Bio* 2016;**6**:835−46.
15. Meissner L, Gallozzi M, Balbi M, Schwarzmaier S, Tiedt S, Terpolilli NA, et al. Temporal profile of microRNA expression in contused cortex after traumatic brain injury in mice. *J Neurotrauma* 2016;**33**:713−20.
16. Tominaga N, Kosaka N, Ono M, Katsuda T, Yoshioka Y, Tamura K, et al. Brain metastatic cancer cells release microRNA-181c-containing extracellular vesicles capable of destructing blood−brain barrier. *Nat Commun* 2015;**6**:6716.
17. Hu Q, Lyon CJ, Fletcher JK, Tang W, Wan M, Hu TY. Extracellular vesicle activities regulating macrophage- and tissue-mediated injury and repair responses. *Acta Pharm Sin B* 2021;**11**:1493−512.
18. Xie W, Zhou P, Sun Y, Meng X, Dai Z, Sun G, et al. Protective effects and target network analysis of ginsenoside Rg1 in cerebral ischemia and reperfusion injury: a comprehensive overview of experimental studies. *Cells* 2018;**7**:270.
19. Wang R, Wang GJW, Wu XL, Zhou F, Li YN. Ginsenoside Rg1 attenuates structural disruption of the blood−brain barrier to protect the central nervous system in ischemia/reperfusion. *Chin J Nat Med* 2013;**11**:30−7.
20. Lin M, Sun W, Gong W, Ding Y, Zhuang Y, Hou Q. Ginsenoside Rg1 protects against transient focal cerebral ischemic injury and suppresses its systemic metabolic changes in cerebral injury rats. *Acta Pharm Sin B* 2015;**5**:277−84.
21. Wang R, Li YN, Wang GJ, Hao HP, Wu XL, Zhou F. Neuroprotective effects and brain transport of ginsenoside Rg1. *Chin J Nat Med* 2009;**7**:315−20.
22. He C, Feng R, Sun Y, Chu S, Chen J, Ma C, et al. Simultaneous quantification of ginsenoside Rg1 and its metabolites by HPLC−MS/MS: Rg1 excretion in rat bile, urine and feces. *Acta Pharm Sin B* 2016;**6**:593−9.

23. Li Y, Meng Q, Yang M, Liu D, Hou X, Tang L, et al. Current trends in drug metabolism and pharmacokinetics. *Acta Pharm Sin B* 2019;**9**:1113−44.
24. Liu Y, Ou Y, Sun L, Li W, Yang J, Zhang X, et al. Alcohol dehydrogenase of *Candida albicans* triggers differentiation of THP-1 cells into macrophages. *J Adv Res* 2019;**18**:137−45.
25. Neerukonda SN, Egan NA, Patria J, Assakhi I, Tavlarides-Hontz P, Modla S, et al. Comparison of exosomes purified *via* ultracentrifugation (UC) and total exosome isolation (TEI) reagent from the serum of Marek's disease virus (MDV)-vaccinated and tumor-bearing chickens. *J Virol Methods* 2019;**263**:1−9.
26. Sobue A, Ito N, Nagai T, Shan W, Hada K, Nakajima A, et al. Astroglial major histocompatibility complex class I following immune activation leads to behavioral and neuropathological changes. *Glia* 2018;**66**:1034−52.
27. Xiao J, Pan Y, Li X, Yang X, Feng Y, Tan H, et al. Cardiac progenitor cell-derived exosomes prevent cardiomyocytes apoptosis through exosomal miR-21 by targeting PDCD4. *Cell Death Dis* 2016;**7**:e2277.
28. Zhai K, Tang Y, Zhang Y, Li F, Wang Y, Cao Z, et al. NMMHC IIA inhibition impedes tissue factor expression and venous thrombosis *via* Akt/GSK3β-NF-κB signalling pathways in the endothelium. *J Thromb Haemostasis* 2015;**114**:173−85.
29. Zhai KF, Zheng JR, Tang YM, Li F, Lv YN, Zhang YY, et al. The saponin D39 blocks dissociation of non-muscular myosin heavy chain IIA from TNF receptor 2, suppressing tissue factor expression and venous thrombosis. *Br J Pharmacol* 2017;**174**:2818−31.
30. Du M, Giridhar KV, Tian Y, Tschannen MR, Zhu J, Huang CC, et al. Plasma exosomal miRNAs-based prognosis in metastatic kidney cancer. *Oncotarget* 2017;**8**:63703−14.
31. Shi Y, Zhang L, Pu H, Mao L, Hu X, Jiang X, et al. Rapid endothelial cytoskeletal reorganization enables early blood−brain barrier disruption and long-term ischaemic reperfusion brain injury. *Nat Commun* 2016;**7**:10523.
32. Kalra H, Gangoda L, Fonseka P, Chitti SV, Liem M, Keerthikumar S, et al. Extracellular vesicles containing oncogenic mutant β-catenin activate Wnt signalling pathway in the recipient cells. *J Extracell Vesicles* 2019;**8**:1690217.
33. Wang W, Sun J, Wang N, Sun Z, Ma Q, Li J, et al. Enterovirus A71 capsid protein VP1 increases blood−brain barrier permeability and virus receptor vimentin on the brain endothelial cells. *J Neurovirol* 2020;**26**:84−94.
34. Chen HR, Yeh T. *In vitro* assays for measuring endothelial permeability by transwells and electrical impedance systems. *Bio Protoc* 2017;**7**:e2273.
35. Cao GS, Chen HL, Zhang YY, Li F, Liu CH, Xiang X, et al. YiQi-FuMai powder injection ameliorates the oxygen-glucose deprivation-induced brain microvascular endothelial barrier dysfunction associated with the NF-κB and ROCK1/MLC signaling pathways. *J Ethnopharmacol* 2016;**183**:18−28.
36. Ren XS, Tong Y, Qiu Y, Ye C, Wu N, Xiong XQ, et al. MiR155-5p in adventitial fibroblasts-derived extracellular vesicles inhibits vascular smooth muscle cell proliferation *via* suppressing angiotensin-converting enzyme expression. *J Extracell Vesicles* 2020;**9**:1698795.
37. Gao YY, Zhang ZH, Zhuang Z, Lu Y, Wu LY, Ye ZN, et al. Recombinant milk fat globule-EGF factor-8 reduces apoptosis *via* integrin β3/FAK/PI3K/AKT signaling pathway in rats after traumatic brain injury. *Cell Death Dis* 2018;**9**:845.
38. Flierl MA, Stahel PF, Beauchamp KM, Morgan SJ, Smith WR, Shohami E. Mouse closed head injury model induced by a weight-drop device. *Nat Protoc* 2009;**4**:1328−37.
39. AlbertWeißenberger C, Várrallyay C, Raslan F, Kleinschnitz C, Siren AL. An experimental protocol for mimicking pathomechanisms of traumatic brain injury in mice. *Exp Transl Stroke Med* 2012;**4**:1.
40. Jiang B, Li L, Chen Q, Tao Y, Yang L, Zhang B, et al. Role of glibenclamide in brain injury after intracerebral hemorrhage. *Transl Stroke Res* 2017;**8**:183−93.
41. Mann AP, Scodeller P, Hussain S, Joo J, Kwon E, Braun GB, et al. A peptide for targeted, systemic delivery of imaging and therapeutic compounds into acute brain injuries. *Nat Commun* 2016;**7**:11980.
42. Zhai KF, Duan H, Cui CY, Cao YY, Si JL, Yang HJ, et al. Liquiritin from *Glycyrrhiza uralensis* attenuating rheumatoid arthritis *via* reducing inflammation, suppressing angiogenesis, and inhibiting MAPK signaling pathway. *J Agric Food Chem* 2019;**67**:2856−64.
43. Vallon M, Chang J, Zhang H, Kuo CJ. Developmental and pathological angiogenesis in the central nervous system. *Cell Mol Life Sci* 2014;**71**:3489−506.
44. Ping S, Qiu X, Kyle M, Hughes K, Longo J, Zhao LR. Stem cell factor and granulocyte colony-stimulating factor promote brain repair and improve cognitive function through VEGF-A in a mouse model of CADASIL. *Neurobiol Dis* 2019;**132**:104561.
45. Bhalala OG, Srikanth M, Kessler JA. The emerging roles of microRNAs in CNS injuries. *Nat Rev Neurol* 2013;**9**:328−39.
46. Hawkins BT, Davis TP. The blood−brain barrier/neurovascular unit in health and disease. *Pharmacol Rev* 2005;**57**:173−85.
47. Zhang Y, Lv X, Qu J, Zhang X, Zhang M, Gao H, et al. A systematic strategy for screening therapeutic constituents of *Schisandra chinensis* (Turcz.) Baill infiltrated blood−brain barrier oriented in lesions using ethanol and water extracts: a novel perspective for exploring chemical material basis of herb medicines. *Acta Pharm Sin B* 2020;**10**:557−68.
48. Abbott NJ, Patabendige AA, Dolman DE, Yusof SR, Begley DJ. Structure and function of the blood−brain barrier. *Neurobiol Dis* 2010;**37**:13−25.
49. Han L, Jiang C. Evolution of blood−brain barrier in brain diseases and related systemic nanoscale brain-targeting drug delivery strategies. *Acta Pharm Sin B* 2021;**11**:2306−25.
50. Rosenberg GA. Matrix metalloproteinases and their multiple roles in neurodegenerative diseases. *Lancet Neurol* 2009;**8**:205−16.
51. Yang X, Lu W, Hopper CP, Ke B, Wang B. Nature's marvels endowed in gaseous molecules I: carbon monoxide and its physiological and therapeutic roles. *Acta Pharm Sin B* 2021;**11**:1434−45.
52. Ge X, Li W, Huang S, Yin Z, Yang M, Han Z, et al. Increased miR-21-3p in injured brain microvascular endothelial cells after traumatic brain injury aggravates blood−brain barrier damage by promoting cellular apoptosis and inflammation through targeting MAT2B. *J Neurotrauma* 2019;**36**:1291−305.
53. Miller KE, Suter DM. An integrated cytoskeletal model of neurite outgrowth. *Front Cell Neurosci* 2018;**12**:447.
54. Wang Y, Xu Y, Liu Q, Zhang Y, Gao Z, Yin M, et al. Myosin IIA-related actomyosin contractility mediates oxidative stress-induced neuronal apoptosis. *Front Mol Neurosci* 2017;**10**:75.
55. Wang Y, Liu Q, Xu Y, Zhang Y, Lv Y, Tan Y, et al. Ginsenoside Rg1 protects against oxidative stress-induced neuronal apoptosis through myosin IIA-actin related cytoskeletal reorganization. *Int J Biol Sci* 2016;**12**:1341−56.
56. Kumar A, Stoica BA, Loane DJ, Yang M, Abulwerdi G, Khan N, et al. Microglial-derived microparticles mediate neuroinflammation after traumatic brain injury. *J Neuroinflammation* 2017;**14**:47.